Citation for published version:
Okuda, H, Young, R, Wolverson, D, Tanaka, F, Yamamoto, G & Okabe, T 2018, 'Investigating nanostructures in carbon fibres using Raman spectroscopy', *Carbon*, vol. 130, pp. 178-184.
https://doi.org/10.1016/j.carbon.2017.12.108

DOI:
10.1016/j.carbon.2017.12.108

Publication date:
2018

Document Version
Peer reviewed version

Link to publication

Publisher Rights
CC BY-NC-ND

University of Bath

Alternative formats
If you require this document in an alternative format, please contact:
openaccess@bath.ac.uk

General rights
Copyright and moral rights for the publications made accessible in the public portal are retained by the authors and/or other copyright owners and it is a condition of accessing publications that users recognise and abide by the legal requirements associated with these rights.

Take down policy
If you believe that this document breaches copyright please contact us providing details, and we will remove access to the work immediately and investigate your claim.

Download date: 05. Jul. 2024

INVESTIGATING NANOSTRUCTURES IN CARBON FIBRES USING RAMAN SPECTROSCOPY

Haruki Okuda[1,2,4], Robert J. Young[2], Daniel Wolverson[3], Fumihiko Tanaka[1], Go Yamamoto[4] and Tomonaga Okabe[4]

1 Composite Materials Research Laboratories, TORAY Industries, Inc., 1515 Tsutsui, Masaki-cho, Iyo-gun, Ehime, 791-3193, Japan
2 School of Materials, University of Manchester, Grosvenor Street, Manchester, M1 7HS, UK
3 Department of Physics, University of Bath, Claverton Down, Bath, BA2 7AY, UK
4 Department of Aerospace Engineering, Tohoku University, 6-6-01, Aoba-yama, Aoba-ku, Sendai, Miyagi, 980-8579, Japan

ABSTRACT

Nanostructures in the PAN-based carbon fibres were investigated by means of the Raman spectroscopy which was performed using a series of different excitation wavelengths. UV-Raman measurements showed the predominance of sp^2 carbon for the carbon fibres with Young's moduli ranging from 55 to 440 GPa. The excitation wavelength dependence of the spectral line shape implied the presence of the graphitic (sp^2 carbon layers) as well as the amorphous carbon-like component (sp^2 carbon clusters) in these fibres. An analytical model based upon the Tuinstra-Koenig relation and the rule-of-mixtures concept was proposed to account for the observed behaviour of the peak intensity ratio I_D/I_G. It was suggested that the carbonisation heat treatment led to the sp^2 carbon layers extending rapidly throughout the nanostructure, resulting in the complete loss of the sp^2 carbon clusters for the higher-modulus carbon fibres. These new findings together with the proposed analytical model are believed to be essential keys towards the development of new generation carbon fibres.

1 INTRODUCTION

Due to their excellent mechanical performance per weight, polyacrylonitrile (PAN)-based carbon fibres have widely been accepted in a broad range of industrial applications [1]. Throughout the development history of the PAN-based carbon fibres, understanding their structure-property relation has always been one of the central subjects in order to further improve their capabilities. We have recently demonstrated that the mechanical properties of

the PAN-based carbon fibres, such as tensile modulus [2], tensile strength [3,4] and compressive strength [5] can be reasonably explained by assuming carbon fibres being nanocomposites which consist of the crystallites and a disordered part [6-8]. It is therefore thought that clear insights into the detailed structure of these components, in particular the disordered part, is essential for further improving the performance of the PAN-based carbon fibres.

There have already been a number of studies regarding the nanostructure of the carbon fibres based upon a variety of techniques which includes wide-angle X-ray diffraction (WAXD) [9,10], small-angle X-ray scattering (SAXS) [10-13], transmission electron microscope (TEM), selected-area electron diffraction (SAED) [14-16] and Raman spectroscopy [17-20]. As compared to the crystallites, however, the understanding upon the disordered part in the carbon fibres is limited, possibly due to the lack of suitable analytical techniques. Recently, Raman spectroscopy has been applied extensively to a broad range of carbon materials from graphitic [23-25] to amorphous carbon materials [26-29] as a powerful tool to characterise their nanostructure, since each different carbon material shows its own spectral line shape in their Raman spectra. In addition to this, the spectral line shape of the carbon materials changes drastically depending upon the excitation wavelengths and this dependence can be used as a unique fingerprint for identifying the type of carbon materials [23-28]. It is thus expected that both the crystallites and the disordered part in the carbon fibres could be characterised in details by means of the Raman spectroscopy using multiple laser wavelengths. To the best of our knowledge, however, there has been no such report in which Raman spectra have been used to investigate the detailed structure of the each component in the carbon fibres. One of the main reasons for this, we believe, is the lack of an appropriate framework that enables the separation of the contributions from the individual components in the Raman spectra of carbon fibres.

In order to quantitatively analyse the Raman spectra for the carbon fibres, a curve fitting method which is universally applicable to a wide range of carbon fibres is necessary. Various curve fitting methods have proposed in literature so far for the analysis of the Raman spectra of the carbon fibres. Melanitis and coworkers fitted the D, G and D' bands of the Raman spectra for some intermediate- and high-modulus carbon fibres using a set of three Lorentzian functions [17]. Frank applied two Lorentzian functions in order to fit the G band [18]. Vautard *et al.* introduced three Lorentzian functions in order to fit the D, G band and a shoulder around 1100 cm^{-1}, respectively [21]. Zickler *et al.* used five Voigt functions to fit the Raman spectra for a variety of PAN- as well as pitch-based carbon fibres [22]. In these

conventional fitting approaches, the broad spectral line shape of the carbon fibres often requires an additional peak between the D and G bands [22]. For the amorphous carbon materials, this residual intensity adjacent to the G band has been explained as the asymmetric tail of the G band. Several researchers have pointed out that the Breigt-Wigner-Fano (BWF) function successfully reproduces the asymmetric G band of sp^2 carbon materials [26,29]. Considering that the carbon fibres are made up of crystallites and a disordered part, it is expected that the BWF function is also applicable to the curve fitting of the Raman spectra for the carbon fibres.

In this study, the nanostructures of the carbon fibres were investigated by means of the Raman spectroscopy using a series of different excitation wavelengths with an aim of clarifying the key for further improvements the mechanical performance of the PAN-based carbon fibres.

2 EXPERIMENTAL

2.1 Materials

PAN-based carbon fibres that are thought to represent a wide range of different nanostructures were used in this study (Table 1). No surface treatment was applied for these fibre samples after carbonisation or graphitisation to avoid any possible spurious effects due to the changes in the surface structure. Prior to the experiments, fibre samples were washed with acetone at room temperature, followed by the air-drying, to remove any impurities. For the Raman measurements, a small number of fibres were attached on a slide glass with adhesive tape. In order to avoid possible artefact peaks from the slide glass, these fibres were attached with one end being located 5 mm away from an edge of the slide glass as depicted in Fig. 1. These fibre samples were confirmed to show no skin-core differences in their Raman spectra as shown in the supplementary information.

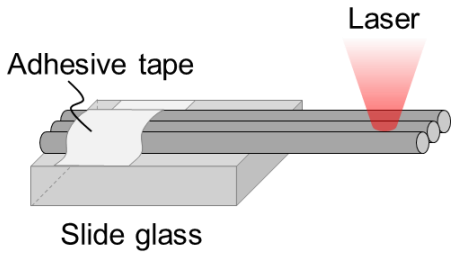

Figure 1: Geometry of the Raman measurements.

Table 1: The physical and the mechanical properties of the carbon fibres studied. The crystallite sizes L_c, L_a, which denote the average thickness of the crystallites, the average diameter of the crystallites parallel to the fibre axis, respectively, and the orientation parameter π_{002} were evaluated using WAXD [10].

	Young's Modulus /GPa	Density /gcm^{-3}	Diameter /μm	L_c /nm	L_a /nm	π_{002} /-
CF13	55	1.57	6.6	1.3	1.3	0.815
CF15	150	1.78	6.2	1.3	1.5	0.815
CF17	200	1.82	6.0	1.3	1.7	0.819
CF19	240	1.78	5.8	1.4	1.9	0.822
CF21	272	1.80	5.7	1.4	2.1	0.823
CF24	294	1.80	5.5	1.3	2.4	0.825
CF27	294	1.80	5.5	1.9	2.7	0.821
CF36	294	1.73	5.6	2.4	3.6	0.845
CF72	380	1.80	5.4	3.7	7.2	0.883
CF100	440	1.85	5.3	4.7	10.0	0.904

2.2 Methods

All the WAXD measurements were performed at the beam line BL03XU/Spring-8 (Frontier Softmaterial Beamline "FSBL") of the Japanese Synchrotron Radiation Facility. The incident beam of the wavelength of 0.08 nm was used to irradiate bundles of about 300 individual fibres. The diffracted beam was captured with a flat panel detector which was positioned at a distance of about 5-10 cm from the fibre bundle. The fibre axis was set perpendicular to the incident beam for the measurement of the 002 reflection, while the angle between the fibre axis and the incident beam was adjusted by about 10-15 º for evaluating the 10 reflection. Measurements were repeated twice and the 2D diffraction patterns thus obtained were averaged. The reflection peak profiles against the 2θ direction were obtained by integrating the 2D reflection patterns with a small azimuthal angle of ±30° and 5° for the 002 and the 10 peaks, respectively. The average thickness L_c and the average diameter of the

crystallites parallel to the fibre axis L_a were evaluated from the peak profiles of the 002 and the 10 reflections, respectively, according to the method of Shioya *et al.* [10]. The orientation parameter π_{002} was calculated from the azimuthal profile of the 002 reflection [10].

Raman spectra for the excitation wavelengths of 830 nm (1.49 eV, IR), 633 nm (1.96 eV) and 514 nm (2.41 eV) were measured using a Renishaw 1000 spectrometer. For 488 nm (2.54 eV) and 325 nm (3.82 eV, UV), a Horiba-Jobin-Yvon LabRam was used. Measurements using 244 nm (5.08eV, deep-UV) were performed using Renishaw 2000 spectrometer. In order to avoid any effect associated with heating, the laser power at fibre surface was adjusted to be less than 3 mW using ND filters. Magnification of the objective lens was 50×, giving a beam spot diameter of around 2 μm [30], throughout the study except for the 325 nm excitation, for which the objective magnification employed was 40×. The incident laser beam was linearly polarised with the polarisation direction always being parallel to the fibre axis. No analyser was used in this study. All the measurements were performed three times and averaged.

In this study, Raman spectra were analysed using a combination of fitting functions which contain a Voigt function, two Gaussian functions and an asymmetric Lorentzian function. Specifically, a Voigt function, Gaussian function and asymmetric Lorentzian function were selected with intention to fit the D, D' and G band, respectively. The remaining Gaussian function was used to account for a shoulder peak at around 1100 cm^{-1}. This package of fitting functions is designed to be applicable to the Raman spectra for a wide range of carbon fibres irrespective of the excitation wavelengths. The asymmetric Lorentzian function has been derived on the basis of the BWF function. Full details are given in the supplementary information.

3 RESULTS

3.1 Excitation wavelength dependence

Fig. 2 summarises the Raman spectra for a series of carbon fibres obtained using 5 different excitation wavelengths λ_{ex} ranging from 830 (IR) to 325 nm (UV). It can be seen that the spectral line shape changes drastically depending upon the fibre type as well as the excitation wavelength. Interestingly, as the excitation wavelength becomes shorter, the D band intensity rapidly diminishes in the case of the high-modulus fibres (CF72 and CF100), whereas that for the other fibre types still remains even for the UV excitation (325 nm). The former behaviour resembles that of graphitic materials [23-25], where the change in the

relative intensity of the D band against the G band was explained to be due to the different excitation energy dependence of the Raman cross sections for these bands [24]. The similar dependence upon the excitation wavelength for the high modulus fibres suggests that these fibres predominantly consist of the sp^2 carbon layers. The residual D band for the rest of fibres (CF13 to CF36) is, on the other hand, similar to the behaviour which was reported for sputtered amorphous carbon (*a*-C) films [27,28]. Taking into account that sputtered *a*-C is thought to consist of clusters of small sp^2 carbon layer fragments, chains and rings, it would be expected that the carbon fibres which showed the D band in the UV-Raman spectra (325 nm) contain similar sp^2 carbon clusters. The results that the PAN-based carbon fibres are predominantly consisted of the sp^2 carbons are further supported by using the deep-UV excitation (244 nm). Fig. 3 shows the excitation wavelengths-dependence of the Raman spectra for CF27 and CF100 which were chosen to represent the intermediate- and the high-modulus type fibres, respectively. Even when the deep-UV excitation (244 nm) was applied, neither of the fibres showed T band at around 1100 cm^{-1} which arises from the sp^3 hybridised carbon [32]. It is clear from all the above that, by applying multiple excitation wavelengths, it can be shown that PAN-based carbon fibres are composed exclusively of sp^2 carbon, being mixtures of sp^2 carbon layers and sp^2 carbon clusters.

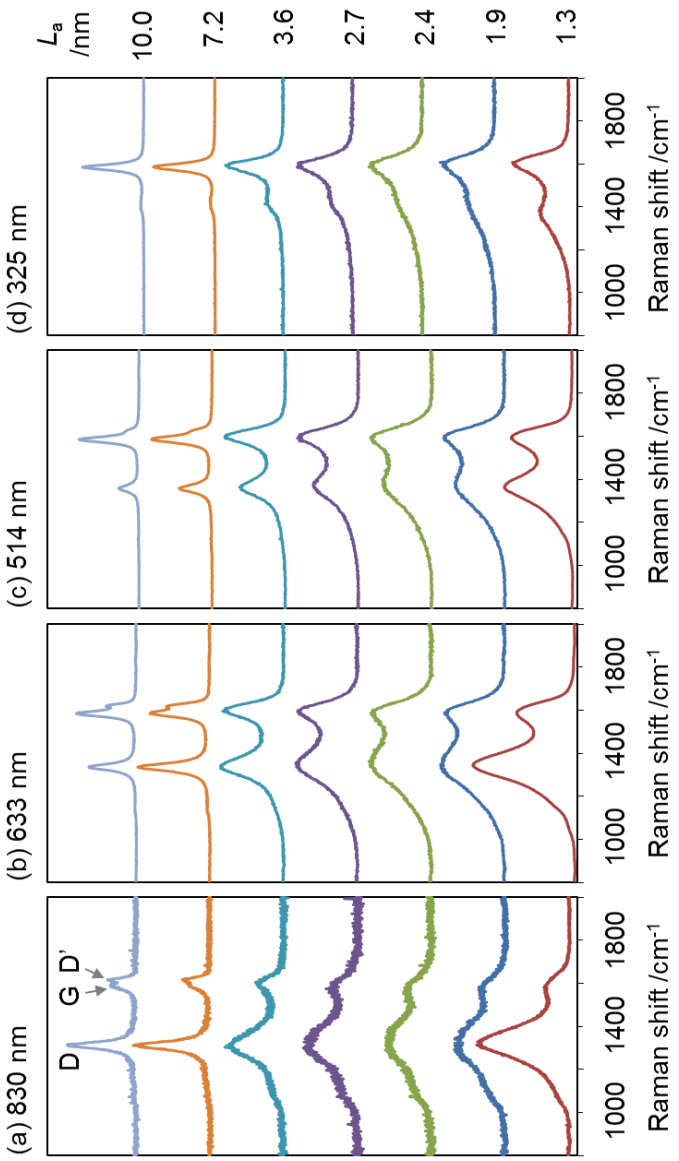

Figure 2: Raman spectra of carbon fibres for different excitation wavelengths λ_{ex} : (a) 830 nm, (b) 633 nm, (c) 514 nm and (d) 325 nm. All the spectra were normalised according to the G band intensities.

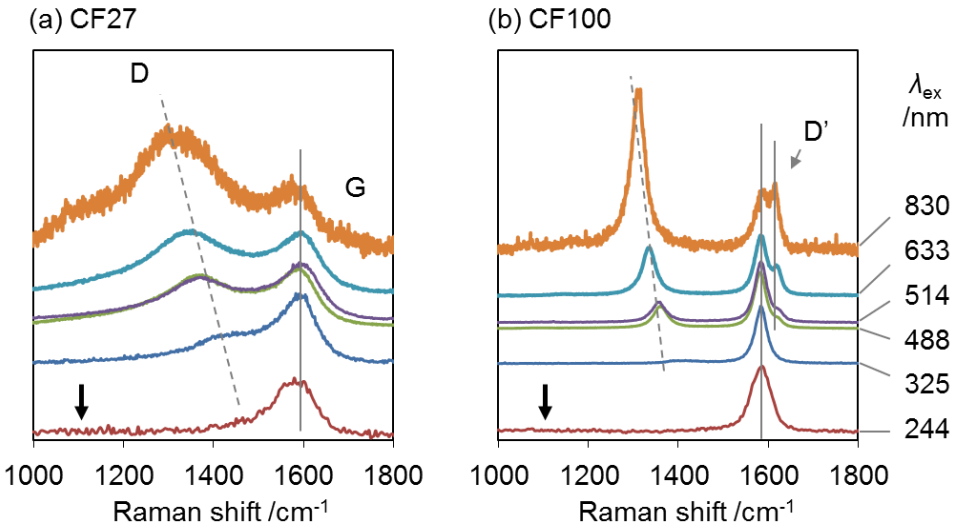

Figure 3: Raman spectra of carbon fibres for different excitation wavelengths λ_{ex} : (a) CF27 and (b) CF100. Arrows show the expected position of the T band in the presence of the sp^3 carbon.

3.2 Peak assignments

The application of the multiple excitation wavelengths in the Raman spectroscopy for the analysis of PAN-based carbon fibres not only suggests that the carbon fibres consist of sp^2 carbon layers and sp^2 carbon clusters but also gives a new insight into the origins of the Raman D and G bands for these materials. Taking into account that the crystallite sizes L_a in the carbon fibres studied in this work are relatively small, ranging from 1.3 to 10.0 nm, the sp^2 carbon layers in these fibres should contain certain amounts of the "edge" carbons. It is therefore expected that these fibres show both the D and G bands as in the case of the microcrystalline graphite [28,31]. Meanwhile, it was reported that the sputtered *a*-C displays both the G and D bands [27,28]. It would therefore be reasonable to expect for the sp^2 carbon clusters in the PAN-based carbon fibres to show both bands. Hence, we propose that the Raman spectra of PAN-based carbon fibres are essentially the superposition of the spectra for the sp^2 carbon layers and the sp^2 carbon clusters as shown in Fig. 4.

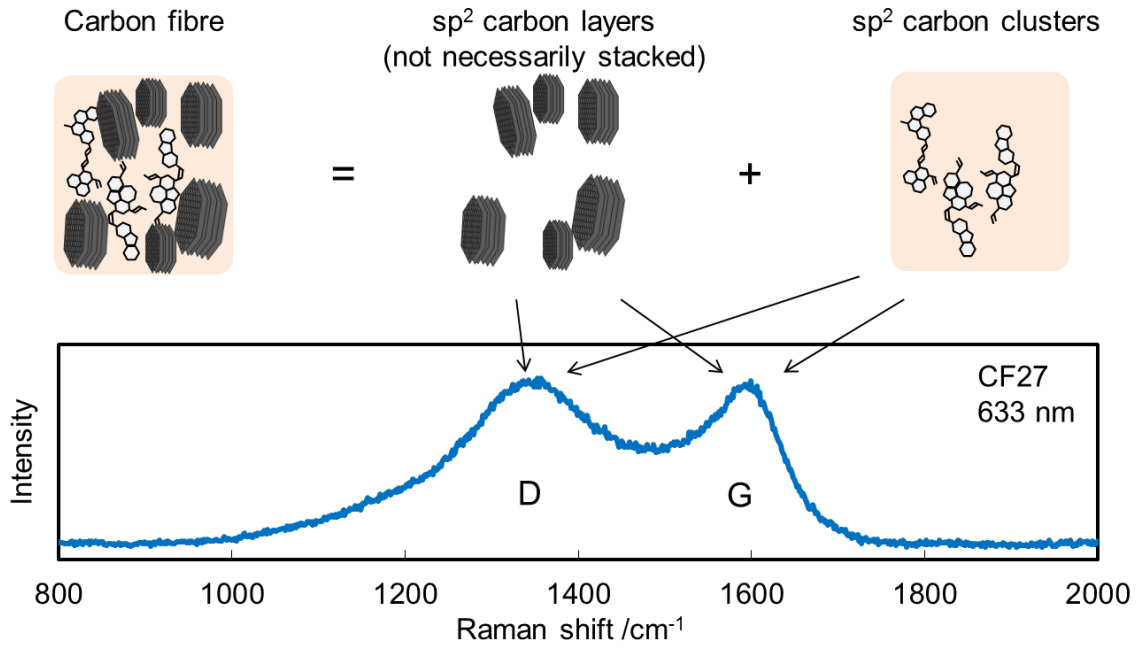

Figure 4: Peak assignments of the Raman spectra based on the plausible nanostructure of PAN-based carbon fibres.

3.3 Tuinstra-Koenig relation

It is interesting to see if the Tuinstra-Koenig relation [20], which has been utilised widely to analyse the Raman spectra of a broad range of carbon materials, could still be applicable to the carbon fibres even though they are the mixtures of sp^2 carbon layers and sp^2 carbon clusters. The relation is given as follows.

$$\frac{I_D}{I_G} = c(\lambda_{ex})\frac{1}{L_a} \tag{1}$$

where $c(\lambda_{ex})$ is a constant that depends upon the excitation wavelength λ_{ex}. The peak intensities I_D and I_G of the D and G band, respectively, were calculated with respect to their integrated areas. Fig. 5 and 6 illustrate the fitting results of the Raman spectra for CF27 and CF100, respectively. It can be seen that the Raman spectra for CF27, which shows broad spectral line shapes, can be fitted reasonably well using the set of fitting functions proposed in the experimental section irrespective of the excitation wavelengths (Fig. 5). Similarly, Fig. 6 demonstrates that the same combination of the fitting functions can also be applied without

any correction to the Raman spectrum of CF100, which represents high-modulus type carbon fibres. The values of the peak intensity ratio I_D/I_G were then obtained for all the carbon fibres studied.

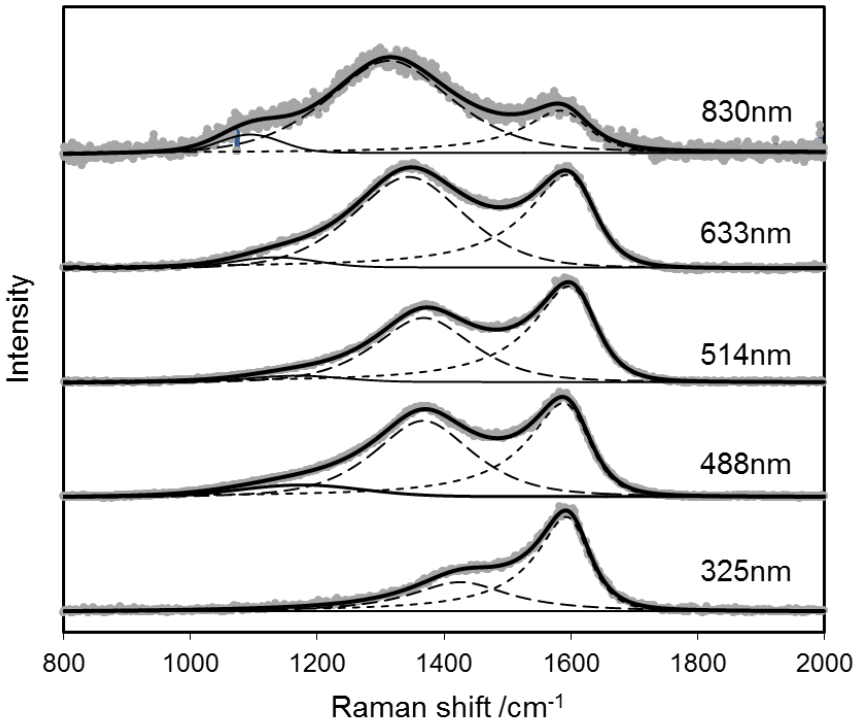

Figure 5: The Raman spectra for CF27 obtained using a series of the excitation wavelengths fitted with the combination of the fitting functions used in this study.

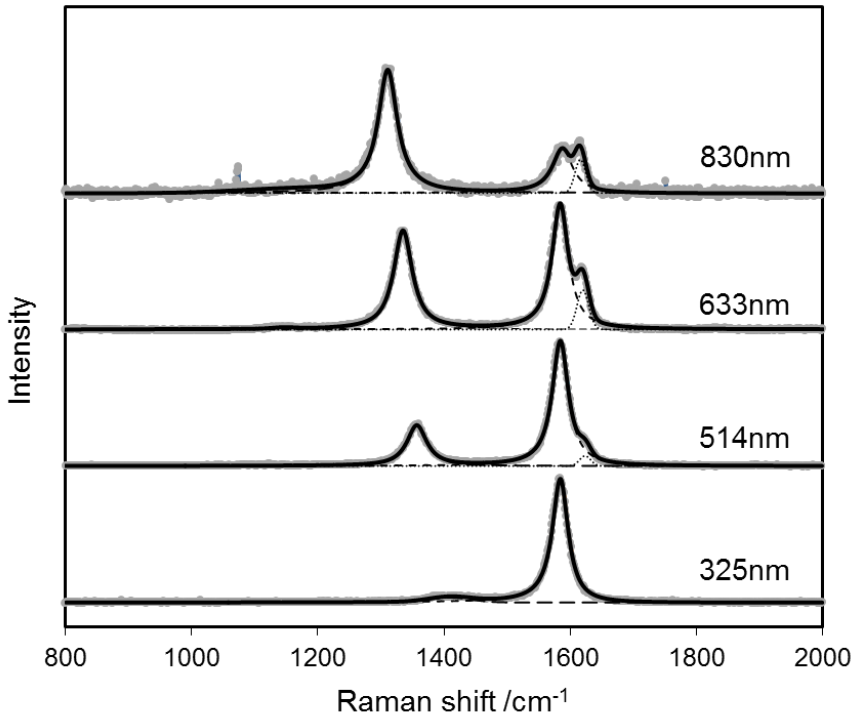

Figure 6: The Raman spectra for CF100 obtained using a series of the excitation wavelengths fitted with the combination of the fitting functions used in this study.

The peak intensity ratio I_D/I_G was plotted against the crystallite size L_a as shown in Fig. 7. The straight lines in Fig. 7 represent the Tuinstra-Koenig relation given by eq. 1. The values for the constant $c(\lambda_{ex})$ were arbitrarily adjusted to let each straight line pass through the experimental value for CF100 (L_a = 10.0 nm) . It can clearly be seen that, for the fibres in which the crystallite size L_a is below several nano-meters, irrespective of the excitation wavelength employed, the observed values (symbols) deviate from the Tuinstra-Koenig relation (lines). Surprisingly, the UV excitation (325 nm) gave an anomalous upward deviation from the Tuinstra-Koenig relation. To the best of our knowledge, this anomalous behaviour has not been pointed out in the literature so far. The other wavelengths, on the other hand, resulted in downward shifts as have been reported for the other carbon materials [22,26]. Considering that the observed spectra originate from both the sp^2 carbon layers and the sp^2 carbon clusters, these deviations from the Tuinstra-Koenig relation could be due to the basic architecture of the carbon fibres as nanocomposites [2-5].

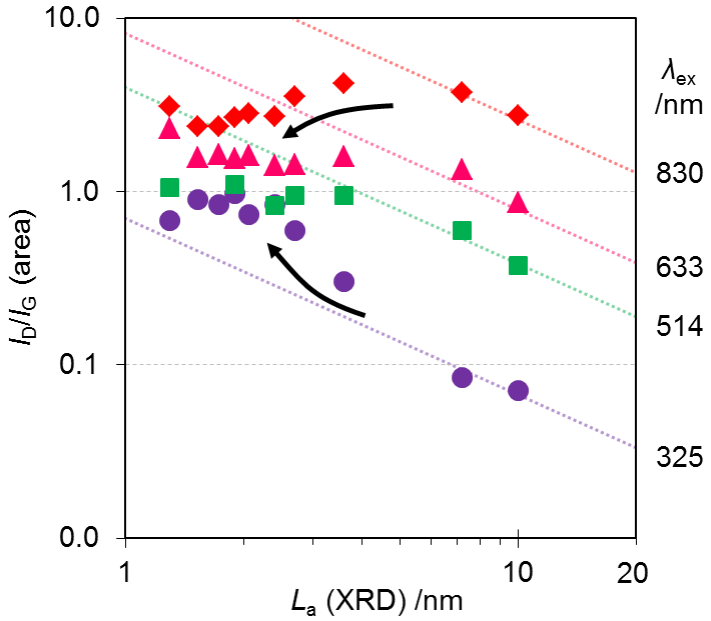

Figure 7: Relation between the crystallite size L_a and the Raman band intensity ratio I_D/I_G. The dotted lines are guide for eyes to show the L_a^{-1} dependence (Tuinstra-Koenig relation).

4 DISCUSSION

4.1 Reconsideration of I_D/I_G ratios for carbon fibres

Assuming that the Raman spectra of carbon fibres are the superposition of the spectra for the sp^2 carbon layers and the sp^2 carbon clusters as discussed above, the observed intensities I_G^{obs} and I_D^{obs} may be expressed using the rule-of-mixtures as

$$I_G^{obs} = fI_G^{c} + (1-f)I_G^{d} \quad (2)$$

$$I_D^{obs} = fI_D^{c} + (1-f)I_D^{d} \quad (3)$$

where f, I_G^c, I_G^d, I_D^c and I_D^d denote the weight fraction of the sp^2 carbon layers, the G band intensity of the sp^2 carbon layers, the G band intensity of the sp^2 carbon clusters, the D band intensity of the sp^2 carbon layers and the D band intensity of the sp^2 carbon clusters, respectively. In addition, it should be mentioned here that the band intensities are based on the area rather than the height. The observed band intensity ratio may then be expressed as

$$\left(\frac{I_D}{I_G}\right)^{obs} = \frac{f{I_D}^c + (1-f){I_D}^d}{f{I_G}^c + (1-f){I_G}^d} \tag{4}$$

with respect to graphene and graphite, Cançado *et al.* have shown experimentally that the intensity ratio I_D/I_G scales with the -4th power of the excitation energy E_{ex} [23-25]. The sp^2 carbon layers in the carbon fibres may scale in the same way

$$\frac{{I_D}^c}{{I_G}^c} = \alpha {L_a}^{-1} {E_{ex}}^{-4} \tag{5}$$

where α and L_a denote a constant and the crystallite size evaluated using XRD, respectively. The constant α depends upon the type of the material and the experimental conditions. Since the peak intensity ratio I_D/I_G for the different amorphous carbon scales differently depending on the type of the material [27,28] and is independent of the crystallite size, the intensity ratio I_D/I_G for the sp^2 carbon clusters in carbon fibres would be expressed as

$$\frac{{I_D}^d}{{I_G}^d} = \beta {E_{ex}}^{-m} \tag{6}$$

where β and m denote a constant and the power law exponent of the excitation energy dependence, respectively. The constant β will depend upon the type of the material and the experimental conditions. The G band intensity for the sp^2 carbon layers can be assumed to be linearly proportional to that for the sp^2 carbon clusters with γ being a proportional constant as follows

$${I_G}^c = \gamma {I_G}^d \tag{7}$$

Ferrari *et al*. suggested that the G band arises from pairs of sp^2 carbon atoms and its intensity is not sensitive to the structural disorder unless sp^3 carbon is introduced [26]. Since there should only be a negligible amount of sp^3 carbon in the PAN-based carbon fibres as

discussed above, the proportional constant γ may be approximated as ~1. Combining eqs. 2-7 gives a modified formulation of the Tuinstra-Koenig relation as follows, which takes into account the nature of carbon fibres as nanocomposites

$$\left(\frac{I_D}{I_G}\right)^{obs} = \left(\alpha L_a^{-1} E_{ex}^{-4} - \beta E_{ex}^{-m}\right) f + \beta E_{ex}^{-m} \quad (8)$$

4.2 Application of the modified Tuinstra-Koenig relation

In order to understand the reason for the anomalous behaviour of the peak intensity ratio I_D/I_G and characterise the nanostructure of the PAN-based carbon fibres, the modified Tuinstra-Koenig relation (eq. 8) was applied to the experimental results shown in Fig. 7. Upon fitting the experimental values with eq. 8, it was assumed that the parameters α, β and m are independent of the fibre type and the weight fraction of the sp^2 carbon layers f depends upon the fibre type. The excitation energy E_{ex} was calculated from the excitation wavelength λ_{ex} as $E_{ex} = 1240/\lambda_{ex}$. The results are summarised in Fig. 8. It can be seen that the experimental values are reproduced by the modified Tuinstra-Koenig relation (eq. 8) reasonably well. The fitting parameters α, β and m were determined to be 124 nm eV^4, 0.9 eV^0 and 0, respectively. The weight fraction of the sp^2 carbon layers f was estimated as shown in Fig. 9, which will be discussed later. With respect to the parameter α, the value of 124 nm eV^4 found in this analysis is close to those reported for nano-graphite [23,24] and monolayer graphene [25] by Cançado *et al*., which are 160 and 560 nm eV^4, respectively. Meanwhile, the power law exponent m was estimated to be 0, which suggests that the peak intensity ratio I_D/I_G of the sp^2 carbon clusters is insensitive to the excitation wavelength. According to the experimental results reported by Ferrari and Robertson [27,28], the excitation energy dependence of the peak intensity ratio for the amorphous carbon is lower than that of the graphitic materials. In specific, the power law exponent m for the sputtered *a*-C film can be estimated from their results to be around 1. This is similar to the value obtained in this study for the sp^2 carbon clusters in the PAN-based carbon fibres. Considering all the above, it is believed that the modified Tuinstra-Koenig relation (eq. 8) is properly representing the physical background of the anomalous behaviour of the peak intensity ratio I_D/I_G. In other words, the concept that the PAN-based carbon fibres as nano-composites built up from the sp^2 carbon layers and sp^2 carbon clusters is confirmed as being reasonable.

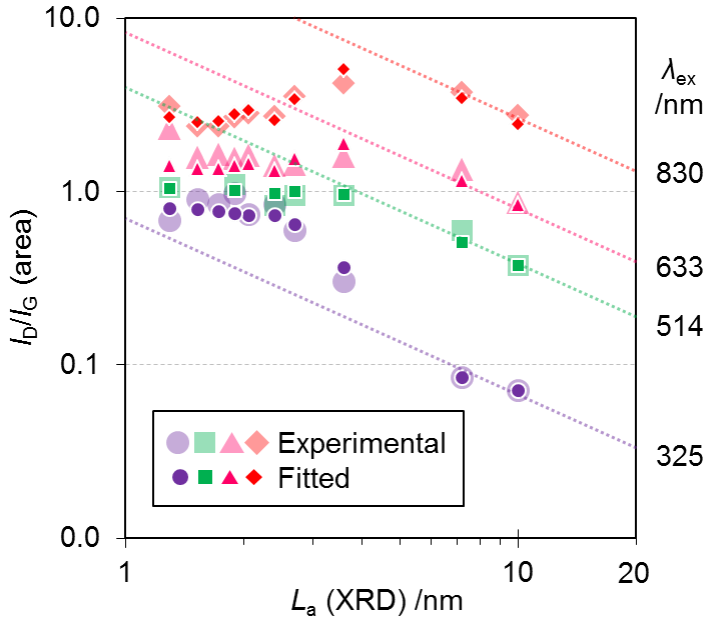

Figure 8: The experimental (larger symbols) and the calculated (smaller symbols) peak intensity ratio I_D/I_G for the series of PAN-based carbon fibres in Fig. 7.

Fig. 9 shows the weight fraction of the sp^2 carbon layers f for the carbon fibres investigated in this study. The weight fraction f increases as the crystallite size L_a increases and then reaches unity at around L_a ~4 nm. Interestingly, the weight fraction of the sp^2 carbon layers f evaluated in this study behaves differently to the crystallite fraction estimated based upon the WAXD analysis. According to Shioya *et al.*, for instances, the crystallite fraction evaluated on the basis of the intensity of the 002 reflection increases monotonically from 0.4 to 0.7 as the crystallite size L_a increases from 2 to 11 nm [9]. It should be remembered that the sp^2 carbon layers detected using Raman spectroscopy reflect the in-plane vibrational mode, whereas the "crystallites" in the WAXD analysis are based upon the out-of-plane stacking of the sp^2 carbon layers. Taking this into consideration, it is thought that the development of the crystallites, or the stacking of the sp^2 carbon layers, is preceded by the extension of the sp^2 carbon layers in the in-plane direction. This could result in an extended network of the sp^2 carbon layers in the PAN-based carbon fibres. We believe that this nano-structural continuity through the sp^2 carbon layers is one of the key structural features that lead to the excellent mechanical performance, particularly the tensile strength, of the PAN-based carbon fibres. Further quantitative studies are necessary to clarify fully the effect of the continuity of the sp^2 carbon layers upon the tensile strength, by means of, for instance, molecular dynamics simulations. In addition, the potential role and the detailed structure of

the sp^2 carbon clusters should be further studied. These aspects will be the subject of our future work. Nevertheless, the above mentioned new insight into the nanostructures represents an important implication for further improving the mechanical performance of PAN-based carbon fibres.

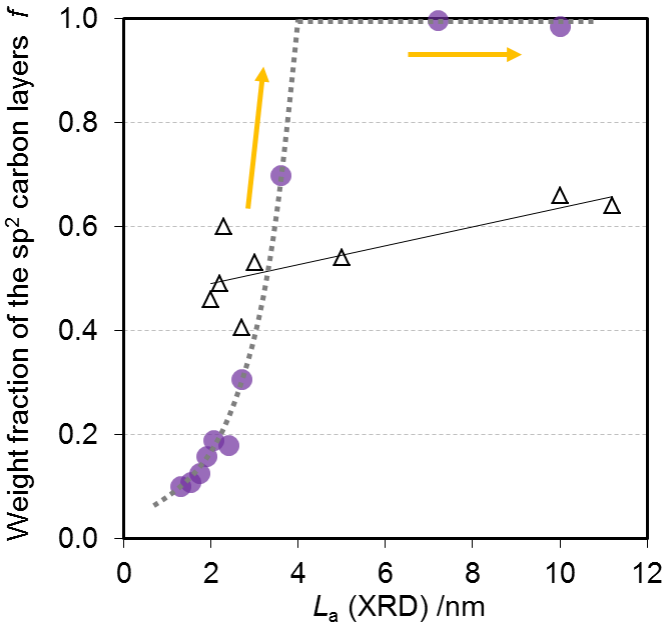

Figure 9: The relation between the crystallite size L_a and: (circles) the weight fraction of the sp^2 carbon layers f estimated in this study, (triangles) the crystallite fraction evaluated on the basis of the 002 reflection [9].

5 CONCLUSIONS

Nanostructures in the PAN-based carbon fibres were investigated by means of the Raman spectroscopy which was performed using a series of different excitation wavelengths.

- From visual inspection of the excitation wavelength dependence of the Raman spectra, it was found that the PAN-based carbon fibres could be regarded as nanocomposites that are made of the sp^2 carbon layers and the sp^2 carbon clusters.

- An analytical model based upon the Tuinstra-Koenig relation and the rule-of-mixture concept was proposed. This model was able to reproduce the experimental behaviour of the peak intensity ratio I_D/I_G reasonably well.

- It was concluded that a rapid increase in the weight fraction of the sp^2 carbon layers precedes the stacking of these layers, and the formation of the crystallites, in the course of the carbonisation heat treatment.
- We believe that this preceding in-plane growth of the sp^2 carbon layers gives a vital continuity in the nanostructure of the PAN-based carbon fibres, leading to their excellent mechanical performance.

REFERENCES

[1] Holmes M. Global carbon fibre market remains on upward trend. *Reinf Plast* 2014;58:38–45.

[2] Tanaka F, Okabe T, Okuda H, Ise M, Kinloch IA, Mori T and Young RJ. The effect of nanostructure upon the deformation micromechanics of carbon fibres. *Carbon* 2013;52:372–8. doi:10.1016/j.carbon.2012.09.047.

[3] Tanaka F, Okabe T, Okuda H, Kinloch IA and Young RJ. Factors controlling the strength of carbon fibres in tension. *Compos Part A Appl Sci Manuf* 2014;57:88–94. doi:10.1016/j.compositesa.2013.11.007.

[4] Okuda H, Young RJ, Tanaka F, Watanabe J and Okabe T. Tensile failure phenomena in carbon fibres, *Carbon* 2016;107:474-481. doi:10.1016/j.carbon.2016.06.037.

[5] Tanaka F, Okabe T, Okuda H, Kinloch IA and Young RJ. The effect of nanostructure upon the compressive strength of carbon fibres. *J Mater Sci* 2012;48:2104–10. doi:10.1007/s10853-012-6984-z.

[6] Loidl D, Peterlik H, Müller M, Riekel C and Paris O. Elastic moduli of nanocrystallites in carbon fibers measured by in-situ X-ray microbeam diffraction. *Carbon* 2003;41:563–70. doi:10.1016/S0008-6223(02)00359-7.

[7] Loidl D, Paris O, Burghammer M, Riekel C and Peterlik H. Direct Observation of Nanocrystallite Buckling in Carbon Fibers under Bending Load. *Phys Rev Lett* 2005;95:225501. doi:10.1103/PhysRevLett.95.225501.

[8] Loidl D, Peterlik H, Paris O, Müller M, Burghammer M and Riekel C. Structure and mechanical properties of carbon fibres: a review of recent microbeam diffraction studies with synchrotron radiation. *J Synchrotron Radiat* 2005;12:758–64. doi:10.1107/S0909049505013440.

[9] Shioya M and Takaku A. Characterization of crystallites in carbon fibres by wide-angle X-ray diffraction. *J Appl Cryst* 1989;22:222-230. doi:10.1107/S0021889888014256

[10] Takaku A and Shioya M. X-ray measurements and the structure of polyacrylonitrile- and pitch-based carbon fibres. *J Mater Sci* 1990;25:4873–9. doi:10.1007/BF01129955.

[11] Perret R and Ruland W. Single and multiple X-ray small-angle scattering of carbon fibres. *J Appl Crystallogr* 1969;2:209–18.

[12] Shioya M and Takaku A. Disorder in the layer stacking in carbon fibers. *Carbon* 1990;28:165–8.

[13] Paris O, Loidl D, Peterlik H, Muller M, Lichtenegger H and Fratzl P. The internal structure of single carbon fibers determined by simultaneous small-and wide-angle scattering. *J Appl Crystallogr* 2000;33:695–9.

[14] Johnson DJ, Crawford D and Jones BF. Observations of a three-phase structure in high-modulus PAN-based carbon fibres. *J Mater Sci* 1973;8:286–90.

[15] Guigon M, Oberlin A and Desarmot G. Microtexture and structure of some high tensile strength, PAN-base carbon fibres. *Fibre Sci Technol* 1984;20:55–72.

[16] Guigon M, Oberlin A and Desarmot G. Microtexture and structure of some high-modulus, PAN-base carbon fibres. *Fibre Sci Technol* 1984;20:177-198. doi:10.1016/0015-0568(84)90040-X

[17] Melanitis N, Tetlow PL and Galiotis C. Characterization of PAN-based carbon fibres with laser Raman spectroscopy. *J Mater Sci* 1996;31:851–60. doi:10.1007/BF00352882.

[18] Frank O, Tsoukleri G, Riaz I, Papagelis K, Parthenios J, Ferrari AC, Geim AK, Novoselov KS and Galiotis C. Development of a universal stress sensor for graphene and carbon fibres. *Nat Commun* 2011;2:255. doi:10.1038/ncomms1247.

[19] Huang Y and Young RJ. Effect of fibre microstructure upon the modulus of PAN- and pitch-based carbon fibres. *Carbon* 1995;33:97–107. doi:10.1016/0008-6223(94)00109-D.

[20] Tuinstra F and Koenig JL. Characterization of Graphite Fiber Surfaces with Raman Spectroscopy. *J Compos Mater* 1970;4:492–9. doi:10.1177/002199837000400405.

[21] Vautard F, Ozcan S, Paulauskas F, Spruiell JE, Meyer H and Lance MJ. Influence of the carbon fiber surface microstructure on the surface chemistry generated by a thermo-chemical surface treatment. *Appl Surf Sci* 2012;261:473–80. doi:10.1016/j.apsusc.2012.08.038.

[22] Zickler GA, Smarsly B, Gierlinger N, Peterlik H and Paris O. A reconsideration of the relationship between the crystallite size L_a of carbons determined by X-ray diffraction and Raman spectroscopy. *Carbon* 2006;44:3239–46. doi:10.1016/j.carbon.2006.06.029.

[23] Cançado LG, Takai K, Enoki T, Endo M, Kim Y, Mizusaki H, Jorio A, Coelho LN, Magalhães-Paniago R and Pimenta MA. General equation for the determination of the crystallite size L_a of nanographite by Raman spectroscopy. *Appl Phys Lett* 2006;88:1–4. doi:10.1063/1.2196057.

[24] Cançado LG, Jorio A and Pimenta M. Measuring the absolute Raman cross section of nanographites as a function of laser energy and crystallite size. *Phys Rev B - Condens Matter Mater Phys* 2007;76:1–7. doi:10.1103/PhysRevB.76.064304.

[25] Cançado LG, Jorio A, Ferreira EHM, Stavale F, Achete CA, Capaz RB, Moutinho MVO, Lombardo A, Kulmala TS and Ferrari AC. Quantifying Defects in Graphene via Raman Spectroscopy at Different Excitation Energies. *Nano Lett*. 2011;11:3190–3196.

[26] Ferrari AC and Robertson J. Interpretation of Raman spectra of disordered and amorphous carbon. *Phys Rev B* 2000;61:14095.

[27] Ferrari AC and Robertson J. Resonant Raman spectroscopy of disordered, amorphous, and diamondlike carbon. *Phys Rev B* 2001;64:1–13. doi:10.1103/PhysRevB.64.075414.

[28] Ferrari AC and Robertson J. Raman spectroscopy of amorphous, nanostructured, diamond-like carbon, and nanodiamond. *Philos Trans A Math Phys Eng Sci* 2004;362:2477–512. doi:10.1098/rsta.2004.1452.

[29] Takabayashi S and Takahagi T. Relationship between Raman and XPS analyses of diamondlike carbon films, *The 74th JSAP Autumn Meeting*, 2013.

[30] Li Z, Kinloch IA, Young RJ, Novoselov KS, Anagnostopoulos G, Parthenios J, Galiotis C, Papagelis K, Lu CY and Britnell L. Deformation of Wrinkled Graphene. *ACS Nano* 2015:150320095742007. doi:10.1021/nn507202c.

[31] Pócsik I, Hundhausen M, Koós M and Ley L. Origin of the D peak in the Raman spectrum of microcrystalline graphite. *J Non Cryst Solids* 1998;227-230:1083–6. doi:10.1016/S0022-3093(98)00349-4.

[32] Gilkes KWR, Prawer S, Nugent KW, Robertson J, Sands HS, Lifshitz Y and Shi X. Direct quantitative detection of the sp^3 bonding in diamond-like carbon films using ultraviolet and visible Raman spectroscopy. *J Appl Phys* 2000;87:10. doi: 10.1063/1.372981.